COBEM 2021 26th International Congress of Mechanical Engineering
November 22-26, 2021, Virtual Congress, Brazil

COB-2021-1996
CHALLENGES TO FABRICATE FUNCTIONALLY GRADED RARE EARTH BASED PERMANENT BONDED MAGNETS VIA POWDER-BASED ADDITIVE MANUFACTURING

Fim, R.G.T.
rafael.gitti@posgrad.ufsc.br;

Röhrig, M.
Mechanical Engineering Department, Federal University of Santa Catarina, UFSC, Florianopolis, SC, 88040-001, Brazil
melissa.rohrig@posgrad.ufsc.br;

Riegg, S.
Functional Materials, Institute of Materials Science, Technical University Darmstadt, Darmstadt, Germany
stefan.riegg@tu-darmstadt.de

Schaefer, K.
Functional Materials, Institute of Materials Science, Technical University Darmstadt, Darmstadt, Germany
kilian.schaefer@tu-darmstadt.de

Gutfleisch, O.
Functional Materials, Institute of Materials Science, Technical University Darmstadt, Darmstadt, Germany
oliver.gutfleisch@tu-darmstadt.de

Ahrens, C.H.
Mechanical Engineering Department, Federal University of Santa Catarina, Florianopolis, SC, 88040-001, Brazil
carlos.ahrens@ufsc.br

Wendhausen, P.A.P.
Mechanical Engineering Department, Federal University of Santa Catarina, Florianopolis, SC, 88040-001, Brazil
paulo.wendhausen@ufsc.br

Abstract. *Aiming to create functionally graded materials (FGMs), challenges regarding both intrinsic and microstructural properties are still to be overcome. Particularly, the latter ones are strongly controlled by the elected processing route. In that regard, Additive Manufacturing (AM) emerges as a promising route to produce not only a wide range of geometric features but most importantly to induce a variety of microstructural characteristics. This principle also enables the generation of structures with engineered heterogeneities alongside a particular axis, resulting in a gradual change of properties and functionality. In the case of magnetic materials, for example, it is possible to manipulate the magnetic field lines for a particular configuration or spatial distribution by only creating structures with particular geometries. We propose that a similar effect could be achieved by varying the volumetric fraction of magnetic particles within the as-printed magnetic samples. This idea is inspired by a previous work of our group, in which it was demonstrated that the magnetic properties of Nd-Fe-B bonded magnets obtained via Laser Powder Bed Fusion (LPBF) can be tuned by controlling the volumetric porosity of the as-printed components. By changing the energy deposited over the powder bed, via variations on laser scan speed (LS) values, it was possible to control the porosity level, which varied between 5% and 40% in volume. In this sense, the present work focuses on the obtention of Nd-Fe-B bonded magnets via LPBF, varying the magnetic particle fraction along a preferred direction, producing a variable magnetic field. A mixture composed of 45% vol. PA-12 and 55% vol. Nd-Fe-B isotropic powder (MQP-S-11-9 grade) was laser processed into magnetic samples via the Selective Laser Sintering (SLS) technique. The AM process was carried out by consolidating individual sections of 5 mm height varying the LS values aiming to induce a variation on magnetic particles fraction alongside a particular axis via porosity control.*

Geometrical density measurements revealed that both strategies adopted were capable to induce a certain level of porosity. Although SEM analysis showed a variable porosity level on each printed section, it was not possible to determine where the porosity is located within the as-printed magnets. Magnetic flux density measurements on both surface and cross-section of the as-printed magnetic samples presented that magnetic flux is homogeneous regardless of the building strategy adopted. Thermal effects related to the own LPBF process change the porosity through the volume, assisting the densification process instead of controlling heterogeneities in each designed section.
Keywords: *Nd-Fe-B bonded magnets, functionally graded materials (FGMs), Laser Powder Bed Fusion, Magnetic properties*

1. INTRODUCTION

Functionally graded materials (FGMs) are a class of materials with variable properties in one (or more) particular directions in space induced by the gradual changes in the composition, chemistry, or microstructure (Bohidar *et al*., 2014.; Knopers *et al*. 2005; Liu *et al.* 2017). These graded structures can be present throughout the material or located in certain regions, resulting in components with heterogeneous properties (magnetic, mechanical, thermal, optical, and so on). The manufacturing process is vital for the obtention of the designed microstructure and the resultant gradient scale. FGMs are obtained in form of bulk or thin films/coatings, where is possible to produce gradients on the millimetric scale (Bobbio *et al*.,2017). Additive Manufacturing (AM) technologies, however, enable the obtention of FGMs with unusual geometries, a very hard task to achieve by conventional manufacturing processes.

The layer-by-layer construction principle enables the properties variations in a micrometric scale, giving rise to a wide range of new functionalities. There are several reports of FGMs obtention via Laser-based processes, Filament Deposition Modeling (FDM), Material Jetting (MJ), and Stereolithography (SLA) processes, for a wide class of materials, ranging from metallic materials and alloys to ceramic and composite materials (Bobbio *et al*.,2017).

Towards gradual functionalization, rare-earth (RE) based bonded permanent magnets are promising candidates to be further explored, gathering both functional gradient and geometrical complexity features. The obtention of a functionally graded permanent magnet is gaining momentum with the AM advance as a result of its potential for application in many industrial sectors, but also for the challenges related to functionalization itself.

The manipulation of the stray field to a specific spatial configuration for a given application is a promising feature of functionally graded bonded permanent magnets, especially for sensing devices (Elian and Theuss, 2014). This can be attained by varying the volumetric fraction of magnetic material in a preferred direction, creating such variations. Since remanence (B_r) values are proportional to the fraction of magnetic particles per unit volume, varying the magnetic compound fraction in a controlled way can be an effective strategy for this purpose (McCurrie, 1981; Searle *et al*., 1982).

Huber et al. (2017) reported this strategy, reporting the obtention of Nd-Fe-B bonded magnet via Filament Deposition Modeling (FDM) technique with variable magnetic particles fraction. In this investigation, composite filaments composed of polyamide-12 (Polyking 221-TR) and isotropic Nd-Fe-B spherical powder (MQP-S-11-9 grade, 85% vol.) were extruded using a 3D end-user printer (Code P). Magnetic samples were obtained by varying the fraction of magnetic powder alongside a particular axis, resulting in a stray field with a specific spatial distribution.

Another approach to creating stray fields with specific configurations is to engineer heterogeneities distributed along a particular direction or axis, promoting variations on the volumetric fraction of magnetic powder, altering the magnitude of the resultant magnetic field. Localized areas with more porosity will present reduced values of remanence (Br) and maximum-energy product ((BH)max) since these areas are majorly occupied by voids, diluting magnetic properties. In contrast, denser regions present elevated values of B_r and $(BH)_{max}$ due to the increase in magnetic particles fraction. As-printed components which present variations on density values can produce stray fields with different magnitudes. Controlling the porosity distribution can be an effective approach to generate a stray field with a particular spatial distribution.

On Powder-based AM, such as Laser Powder Bed Fusion (LPBF) technique, porosity level on the as-printed part is very sensitive to both processing conditions (laser, scan, and temperature-related parameters) and powder-related variables (particle morphology, size, and size distribution). In the case of bonded magnets, the binder volumetric fraction employed on the feedstock also plays a key role in porosity elimination mechanisms. The combination of all these variables brings a wide range of combinations that can be explored aiming at the porosity control for functionally graded bonded magnets obtention.

Fim et al. (2020) addressed these features reporting the influence of processing parameters and feedstock composition on the densification process of Nd-Fe-B bonded magnets obtained via Laser Powder Bed Fusion (LPBF). In their work, feedstocks composed of a mixture of polyamide-12 powder (Duraform PA2200, 36 and 45% vol.) and Nd-Fe-B powder (MQP-S-9-8 grade) were laser processed into magnetic samples via Selective Laser Sintering (SLS), where the laser scan speed (LS) varied from 600 to 1400 mm/s. By adjusting the energy deposited over each layer through LS variations, it was possible to control porosity for the same feedstock composition. The as-printed samples were obtained using 36% vol. PA12 presented geometrical density values ranging from r = 3.32 g/cm³ (LS = 1400 mm/s, 35% porosity) to r = 3.91 g/cm³ (LS = 600 mm/s, 24% porosity). Remanence values varied from Br = 298 mT to Br = 363 mT in this order.

Similar trend was observed when the PA12 fraction increased up to 45% vol., where density values varied from ρ = 3.14 g/cm³ (31% porosity) to ρ = 4.33 g/cm³ (5% porosity), for the same LS variation, resulting on B_r = 282 mT and B_r = 385 mT, respectively. The LPBF technique presents the potential to be a novel approach in the obtention of functionally graded bonded magnets. The strategy to control porosity within the volume of the as-printed magnet aiming to generate a variable magnetic field by a Powder-based AM technique was not reported so far.

Inspired by the context, this present work aims to investigate the obtention of functionally graded Nd-Fe-B bonded magnets via LPBF technique. This work addresses the challenges of AM of bonded magnets with a variable fraction of magnetic compound alongside a particular axis to produce a stray field with different spatial distributions.

2. EXPERIMENTAL

Isotropic Nd-Fe-B bonded magnets were obtained via Laser Powder Bed Fusion (LPBF) technique employing a mixture of polyamide-12 powder (45% vol., Duraform PA2200) and commercial isotropic Nd-Fe-B powder (55% vol., MQP-S-11-9 grade) as feedstock. The feedstock was produced via mechanical mixing using a Y mixer, for 60 minutes, immediately before the laser processing. For this investigation, the Selective Laser Sintering (SLS) process was performed on prototype equipment (Alkimat LaserFunde) using a CO_2 laser source (PURI model PRR 100, λ = 10.6 µm) with 100 W maximum output. Further equipment details are described in Baldissera et al (2018) and Fim et al (2020). The feedstock was then placed inside the SLS equipment and preheated for 30 min at 160°C before laser processing beginning.

To induce a variation on porosity level alongside the z-axis (height) on the as-printed magnetic samples, bonded magnets with dimensions of 20x20x20 mm were obtained as follows:

- Four sections with 5 mm height each were consolidated employing different laser scan speed (LS) values, varying from LS = 600 mm/s to LS = 1600 mm/s;
- After the laser processing of a section, the next one was consolidated using a different LS value. This process was repeated until the components were finished.

As previously reported by Fim et al (2020), the energy density (ED) delivered to each layer can be controlled via LS variations. These variations were reported to be an efficient approach to control final porosity on the as-printed component. In this work, two different sample designs were elaborated to evaluate the feasibility to obtain a variable magnetic flux in a particular axis, as seen in Fig. 1.

The first design (from here on called “Sample A”) consisted to print 4 individual sections of 5 mm height varying the LS values from 600 to 1600 mm/s, in this order. The sections were arranged with the gradual variation on LS values, starting at LS = 600 mm/s (bottom section) and ending at LS = 1600 mm/s (top section).

The second design (referred to as “Sample B”) consisted to print the same 4 sections (h = 5 mm) but employing only the maximum and minimum LS values (600 and 1600 mm/s, respectively), where the sections were alternately arranged.

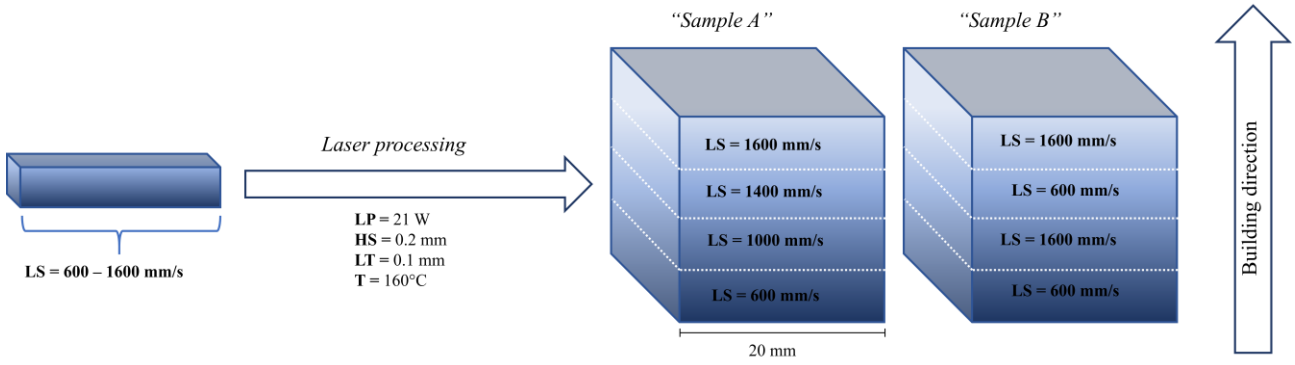

Figure 1: Scheme of the design of the additively manufactured functionally graded bonded magnets.

Table 1: Selective Laser Sintering (SLS) parameters employed on the magnetic samples production.

Laser power, LP (W)	21 W
Hatch spacing, HS (mm)	0.2 mm
Layer thickness, LT (mm)	0.1 mm
Laser scan speed, LS (mm/s)	600 – 1600 mm/s
Printing temperature (°C)	160°C

For comparison, reference samples were produced using the adopted processing conditions (LS = 600 to 1600 mm/s) with different heights, where h = 20 mm (called "Sample C") and h = 5 mm (called "Sample D"). Once the SLS process was completed, the as-printed samples were cooled down to room temperature before removal from the build plate to avoid warpage or geometrical distortions.

Geometrical density measurements from the as-printed samples were carried out to evaluate porosity variations as a function of processing conditions. Scanning Electron Microscopy (Hitachi TM3030) analysis from the fracture surface of both as-printed magnetic samples was carried out to evaluate the final microstructure.

Magnetic flux density and distribution measurements from the samples "A" and "B" were carried out using a custom-built 3D Hall Scanner setup (Technische Universität Darmstadt), which comprises a 3MTS-Sensor (Senis AG, Switzerland) assembled to three linear step motors, each one for individual axis (x, y, and z). The sensor scans the sample surface, measuring the components of the magnetic flux density at every measuring point (Bx, By, and Bz). They control both sensor and stepping motors via LabVIEW software (National Instruments, USA). The 3MTS-Sensor measures a volume of (150x10x150) mm, with ± 1 mT accuracy.

3. PRELIMINARY RESULTS AND DISCUSSION

3.1 Microstructural properties – Geometrical density measurements

Table 1 summarizes the geometrical density measurements results from the as-printed magnetic samples ("A", "B" and references "C" and "D"). Both samples "A" and "B" present the same geometrical density values of $\rho = 3.87$ g/cm³.

Reference samples ("C") produced using LS = 600 – 1400 mm/s presented geometrical density values varying between $\rho = 3.87$ g/cm³ and $\rho = 3.63$ g/cm³, respectively. "Sample D" exhibited slight differences in geometrical density values, which varied between $\rho = 3.87$ g/cm³ and 3.58 g/cm³ for the same LS interval.

Considering a fully dense as-printed bonded magnet, the maximum geometrical density (theoretical density) value achievable can be calculated by the weighted sum of the volumetric fraction of both components employed on the feedstock (PA12 and MQP-S-9-8 powders), according to Eq.1:

$$\rho_{theo} = (\mathbf{f}_{PA12}\, x\, \boldsymbol{\rho}_{PA12}) + (\mathbf{f}_{MQP\text{-}S}\, x\, \boldsymbol{\rho}_{MQP\text{-}S}) \quad (1)$$

Where **f** is the volumetric fraction of each component and **ρ** is the bulk density of both powders, respectively. According to Eq.1, the maximum geometrical density value is $\rho = 4.52$ g/cm³. This represents a porosity degree of $(1 - \rho/\rho_{theo})$ 15% for both "A" and "B" samples, showing that was possible to introduce a similar porosity level by the different adopted strategies. Compared to the "C" samples, densification levels are similar to those obtained employing LS = 600 mm/s but superior to those obtained using LS = 1400 mm/s. Comparing the results to "D" samples, the same trend is observed

The similarity between the geometrical density values from the as-printed samples "A" and "B" can be attributed to the laser processing conditions and associated thermal effects. Despite the different LS employed for each sample, results suggest similar thermal conditions for both strategies.

Table 2: Geometrical density of the as-printed magnetic samples employing different laser scan speed (LS) values.

Sample	Laser scan speed, LS (mm/s)	Geometrical density, ρ (g/cm³)
A	600/1000/1400/1600	3.87
B	600/1600/600/1600	3.87
C	600	3.87
C	1000	3.82
C	1400	3.63
D	600	3.87
D	1000	3.69
D	1400	3.58

In the case of "Sample A", the thermal energy stored during the laser scanning may promote an increase in densification instead of decreasing with LS variations. The bottom layers produced with LS = 600 mm/s were obtained with elevated energy (E_D) density values. The thermal energy accumulated within this volume (20x20x5 mm) allows this section to stay heated, thus assisting the sintering process.

While the next section is being laser processed (LS = 1000 mm/s), the heat stored on the bottom section is dissipated through the new section. This heat dissipation allows the layers obtained with LS = 1000 mm/s remain heated for longer

periods as well, reducing the porosity instead of increasing. As the new section is laser processed (LS = 1400 mm/s), the same phenomenon occurs. This increment in temperature over time deriving from the former laser-scanned layers assists the consolidation phenomena.

With "Sample B", a similar process occurs. The heat stored from the section built using LS = 600 mm/s dissipates through the new section to be consolidated (LS = 1600 mm/s), eliminating part of the porosity intended to be there. When a denser section is built over the porous one using elevated ED values, the thermal energy irradiates through the volume of this section, changing the porosity level. Over time, thermal energy from the top sections irradiates through the volume of the as-printed component, changing the porosity level of the inner sections.

According to Peyre *et al.* (2015), the variation of molten depths presents a linear dependence as a function laser scan speed values. Differences of molten depth from LS = 600 mm/s to LS = 1600 mm/s can cause the unwanted consolidation of the porous section during the laser processing of a denser section above. This can lead to alterations in the porosity level of the porous sections. The different geometrical density values presented by the reference samples reinforce this hypothesis. This is observed when "Sample C" obtained using LS = 1400 mm/s is compared either to "Sample A" and "Sample B", where the geometrical density increases from $\rho = 3.63$ g/cm³ to $\rho = 3.87$ g/cm³, in this order.

The volume of the sample also influences the porosity level of the as-printed parts, evidenced when samples "C" and "D" are compared. The magnetic samples with 20 mm height are denser than 5 mm height, for the same processing conditions (LS = 1000 mm/s and LS = 1400 mm/s). This could be explained by the exposition to less thermal cycles when height is reduced from 20 to 5 mm. This exposition can change the sintering time needed for the polymeric particles to complete the coalescence step, promoting alterations on porosity level. Nonetheless, further exploration is needed.

3.2 Microstructural properties – Scanning Electron Microscopy (SEM) analysis

Figure 2 presents the SEM images from the fracture surface of the as-printed magnetic "Sample B". The building direction is indicated. Fig.2 a represents the bottom section, built using LS = 600 mm/s (elevated energy density). Two main phases are visible and exhibited by the arrows: the magnetic particles (light gray) and the polyamide-12 matrix (dark regions). It is observed the formation of a continuous polymeric matrix, encapsulating a major part of the magnetic particles.

The next section of the as-printed magnet, as shown in Fig. 2 b, represents a porous section of the sample, built using LS = 1600 mm/s (lower energy density). A distinct microstructure is seen, with the absence of a continuous polymeric matrix, with observable pores (dashed circle). Here, only part of the magnetic particles has adhered to the binder due to insufficient time for complete coalescence of polymeric particles, as reported in a previous work (Fim *et al.,* 2020).

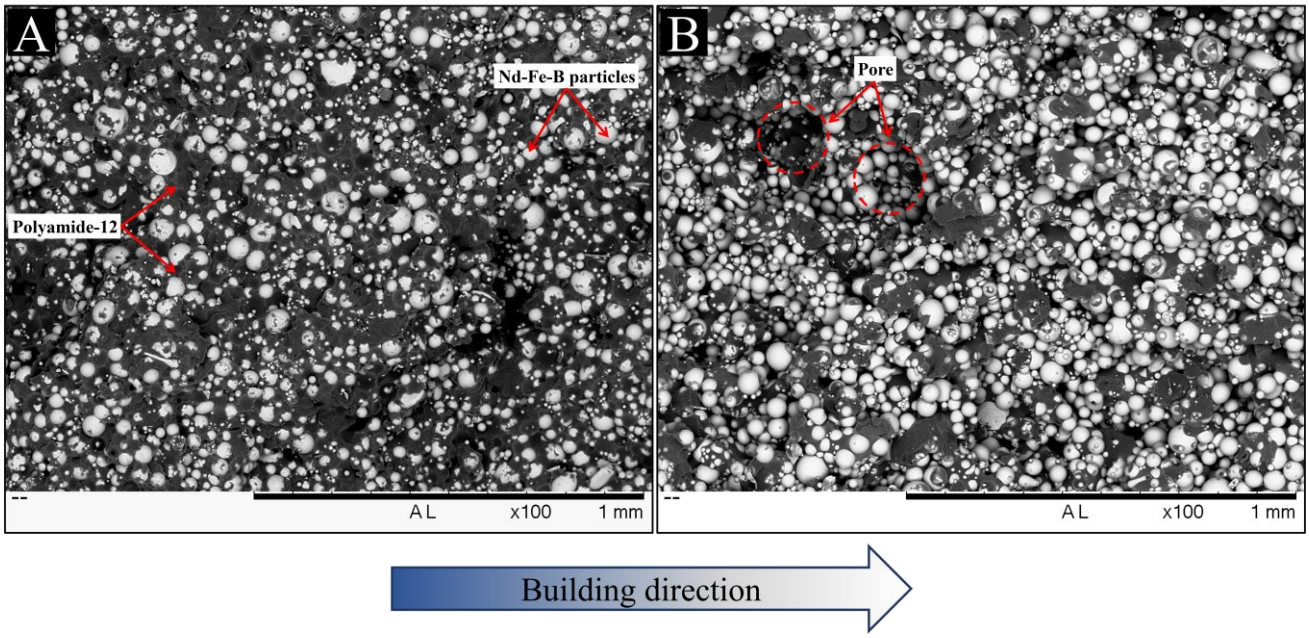

Figure 2: SEM images from the fracture surface of the as-printed "Sample B", where sections were built using (a) LS = 600 mm/s and (b) LS = 1600 mm/s, respectively.

Figure 3-a presents the bottom section of the "Sample A", built employing LS = 600 mm/s. In a similar way as presented in Fig. 2.a, the resultant microstructure presented is also composed by two main phases: the magnetic particles (light gray) and the continuous polymeric matrix (dark regions). The magnetic particles have adhered to the matrix, where the polymer is occupying a great part of the existing voids.

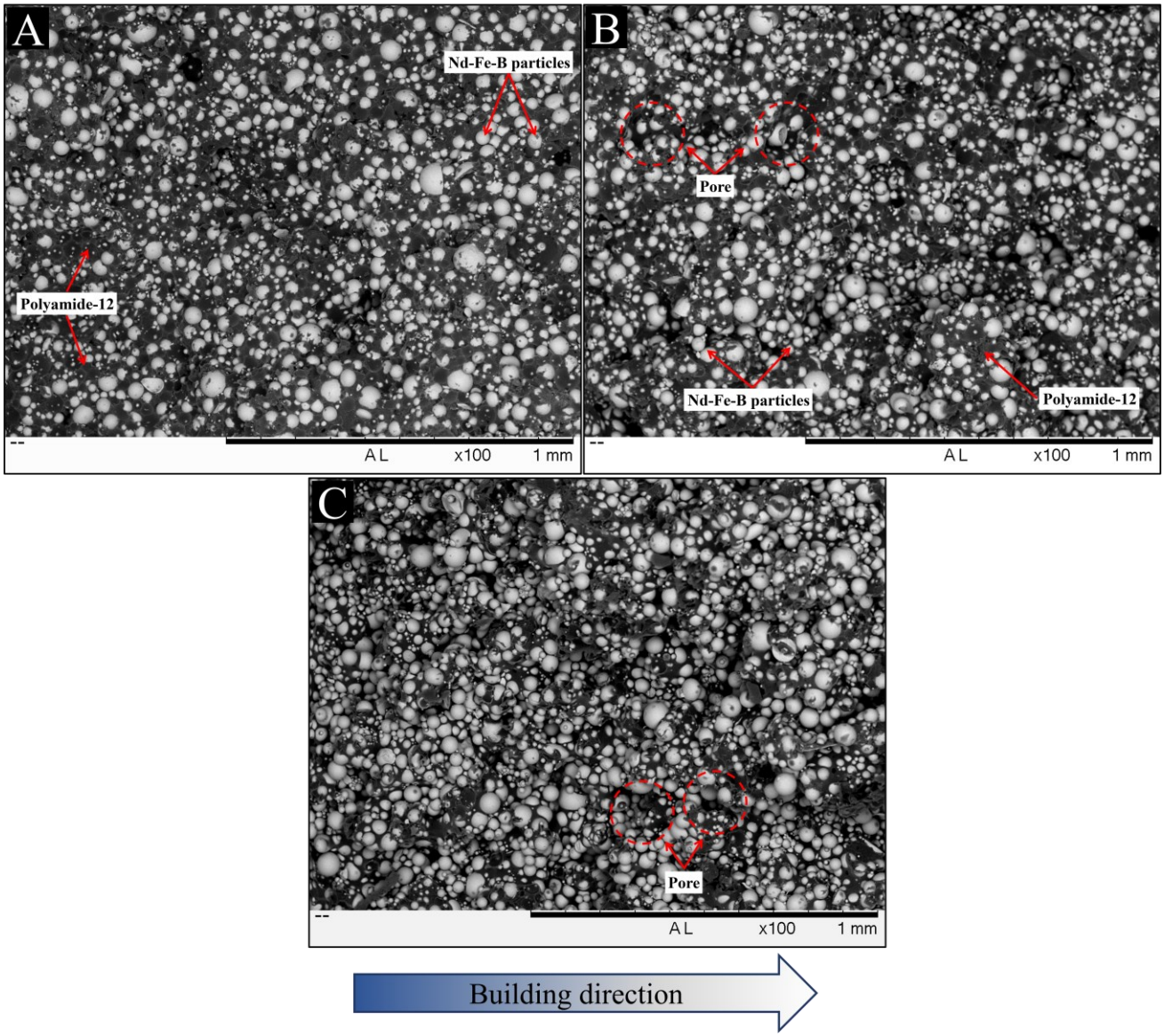

Figure 3: SEM images from the fracture surface of the as-printed "Sample A", where sections were built using (a) LS = 600 mm/s and (b) LS = 1000 - 1400 mm/s and (c) LS = 1600 mm/s, respectively.

In the middle sections, where LS varied between LS = 1000 and 1400 mm/s, the resultant microstructure is very similar in terms of porosity level, as seen in Fig. 3.b. In this section is possible to still observe the presence of the polymeric matrix but now with occurrence of pores (dashed circles). The gradual variation in LS values promotes slight alterations in the microstructure. Increasing the LS values up to LS = 1600 mm/s, the resultant microstructure is presented in Fig. 3 c, where pores are visible once again, without a continuous polymeric matrix. This condition is very similar to the Fig. 2 b.

SEM analysis revealed that the selected building approach was effective to induce a certain porosity level on the as-printed components. However, it was not possible to evaluate if the porosity is homogeneously distributed at each section or if it is concentrated in some regions. As presented earlier, the geometrical density values are similar regardless of the building strategy. Further works will address strategies to better control the porosity level in particular regions of as-printed parts obtained via LPBF.

3.3 Magnetic flux density measurements – functionally graded samples

Fig. 3 presents the magnetic flux density measurements as a function of the position alongside de z-axis from the obtained as-printed magnets, from both "Sample A" and "Sample B". The plotted data presents the z component of magnetic flux as a function of the scanned surface position. The analyzed surface is highlighted by the red dashed area.

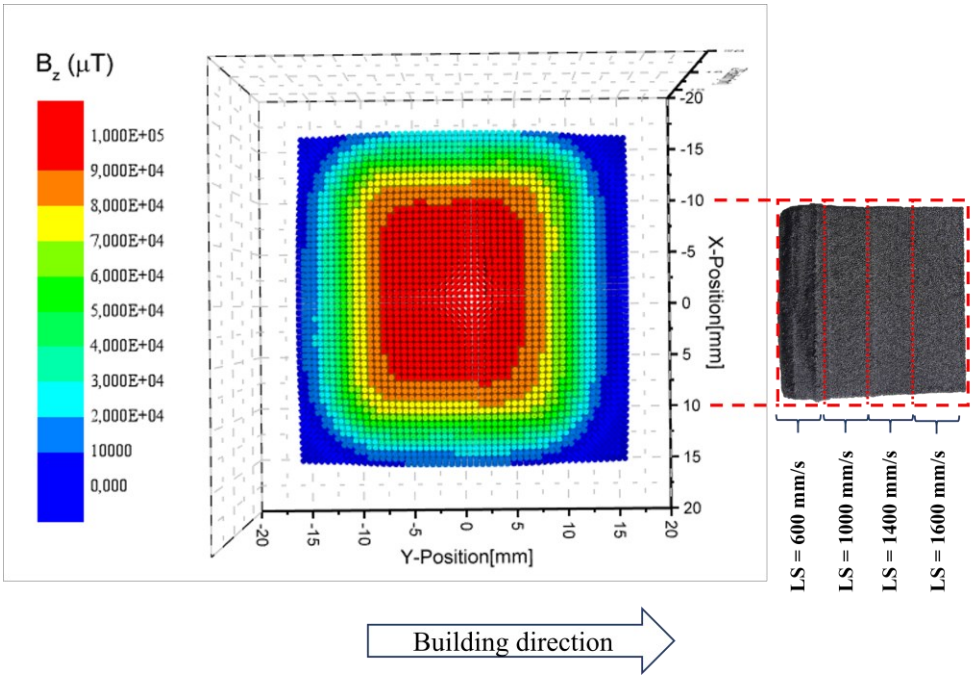

Figure 4: Magnetic flux density measurements as a function of the position alongside the z-axis from the as-printed magnetic sample.

For both as-printed samples ("A" and "B"), the B_z values were homogenous through the analyzed area, where $B_z = 1.10^5$ μT, as seen on the magnetic flux density map in Fig.2. The magnetic flux density measurements indicate that the stray field is homogeneous alongside the building direction (z-axis of the as-printed samples) despite each 5 mm height section was consolidated using different LS values. Stray field intensity variations as a function of position would be expected. However, from geometrical density measurements of both samples ("A" and "B"), it was observed that the laser processing promoted similar densification levels despite the variations on LS values alongside the building direction. The magnetic flux density mapping shows that the resultant porosity is homogeneous alongside the building direction.

Although SEM analysis revealed that it was possible to induce distinct porosity levels alongside the building direction on the as-printed magnetic samples, this porosity was not effective to promote alterations in the magnetic flux. One possibility is the volume alterations of the porous sections due to the laser processing itself. As discussed early, thermal gradients within the printed sections could promote an opposite effect to the porosity distribution along the building direction. Each section was designed to present dimensions of 20x20x5 mm, but after the laser processing, the real volume of each section can be smaller, reducing the effectiveness of the residual porosity on stray field attenuation as a function of the position.

4. SUMMARY AND OUTLOOK

Isotropic Nd-Fe-B bonded magnets were successfully obtained via Laser Powder Bed Fusion (LBPF) employing the cited experimental procedure. The strategy to print sections with 5 mm height each employing different laser scan speed values (LS), ranging from LS = 600 mm/s to LS = 1600 mm/s resulted on as-printed magnetic samples with geometrical density values of $\rho = 3.87$ g/cm³ for both explored approaches. SEM analysis from the fracture surface of the as-printed samples revealed a variable porosity level alongside the building direction. However, it was not possible to determine if the porosity was located homogeneously into each section or if it was located in certain regions. Magnetic flux density measurements carried out at the surface of the samples revealed a homogeneous distribution as a function of the position, indicating that the induced porosity was not effective to induce variations in the stray field. It was hypothesized that thermal effects associated with the laser processing can assist densification instead of retaining the porosity in certain regions of the magnetic samples. Further analysis will help in the comprehension of the obtained results. New printing strategies must be developed for functionally graded bonded magnets obtention via LPBF techniques, considering the particularities of this technique and are elaborated in near future.

5. ACKNOWLEDGEMENTS

The authors would like to thank CNPq and CAPES for the financial support.

6. REFERENCES

Baldissera, A. B., Pavez, P., Wendhausen, P. A. P., Ahrens, C. H. and Mascheroni, J. M. (2017) "Additive Manufacturing of Bonded Nd–Fe–B—Effect of Process Parameters on Magnetic Properties," *IEEE Transactions on Magnetics*, 53(11), pp. 1–4. doi: 10.1109/tmag.2017.2715722.

Bohidar,S.K, Sharma, R., Mishra, P.R, "Functionally graded materials: a critical review", *Int. J. Res*. 1 (4) (2014) 289–301.

Elian, K. and Theuss, H. (2014) "Integration of polymer bonded magnets into magnetic sensors," in *Proceedings of the 5th Electronics System-integration Technology Conference (ESTC*). 2014 Electronics System-Integration Technology Conference (ESTC), IEEE. doi: 10.1109/estc.2014.6962754.

Fim, R. G. T., Mascheroni, A. A., Antunes, L. F., Engerroff, J. B. E., Ahrens, C. H. and Wendhausen, P. A. P. (2020) "Increasing packing density of Additively Manufactured Nd-Fe-B bonded magnets," *Additive Manufacturing*, 35, p. 101353. doi: 10.1016/j.addma.2020.101353.

Gibson, I., Rosen, D., Stucker, B. and Khorasani, M. (2021) *Additive Manufacturing Technologies*. Springer International Publishing

Huber, C., Abert, C., Bruckner, F., Groenefeld, M., Schuschnigg, S., Teliban, I., Vogler, C., Wautischer, G., Windl, R. and Suess, D. (2017) "3D Printing of Polymer-Bonded Rare-Earth Magnets With a Variable Magnetic Compound Fraction for a Predefined Stray Field," *Scientific Reports*, 7(1). doi: 10.1038/s41598-017-09864-0

Knoppers, G., Gunnink, Van Den Hout, W.J., Van Wliet. J, The Reality of Functionally Graded Material Products, Intelligent Production Machines and Systems*, First I* PROMS Virtual Conference: Proceedings and CD-ROM Se*t, Elsevier, 2005, p. 467

Liu, Z. Meyers, M.A. Zhang, Z. Ritchie, R.O., Functional gradients and heterogeneities in biological materials: design principles, functions, and bioinspired applications, *Prog. Mater. Sci*. 88 (2017) 467–498.

McCurrie, R. A. (1981) "Determination of the degree of easy axis alignment in uniaxial permanent magnets from remanence measurements," *Journal of Applied Physics*, 52(12), pp. 7344–7346. doi: 10.1063/1.328725.

Peyre, P., Rouchausse, Y., Defauchy, D. and Régnier, G. (2015) "Experimental and numerical analysis of the selective laser sintering (SLS) of PA12 and PEKK semi-crystalline polymers," *Journal of Materials Processing Technology*, 225, pp. 326–336. doi: 10.1016/j.jmatprotec.2015.04.030.

Searle, C. W., Davis, V. and Hutchens, R. D. (1982) "Magnetically determined particle alignment factors of sintered rare-earth cobalt permanent magnets," Journal of Applied Physics, 53(3), pp. 2395–2397. doi: 10.1063/1.330823.

Zhang, C., Chen, F., Huang, Z., Jia, M., Chen, G., Ye, Y., Lin, Y., Liu, W., Chen, B., Shen, Q., Zhang, L. and Lavernia, E. J. (2019) "Additive manufacturing of functionally graded materials: A review," *Materials Science and Engineering*: A, 764, p. 138209. doi: 10.1016/j.msea.2019.138209.

7. RESPONSIBILITY NOTICE

The author(s) is (are) the only responsible for the printed material included in this paper.